Research Square

Preprints are preliminary reports that have not undergone peer review.
They should not be considered conclusive, used to inform clinical practice,
or referenced by the media as validated information.

TLR3-LCN2 Mediates Microglial M1 Polarization via Iron-ROS Signaling Pathways in Postoperative Cognitive Dysfunction

Xiangyan Jin
Fuzhou University Affiliated Provincial Hospita
Peng Ye
Fuzhou University Affiliated Provincial Hospita
Jingwen Yu
Fuzhou University Affiliated Provincial Hospita
Ming Li
the Affiliated Hospital of North Sichuan Medical College
Yongxin Huang
Fuzhou University Affiliated Provincial Hospita
Ting Zheng
Fuzhou University Affiliated Provincial Hospita
Zhibin Huang
Fuzhou University Affiliated Provincial Hospita
Xin Zhang
920th Hospital of Joint Logistics Support Force, PLA
Xiaochun Zheng
Fuzhou University Affiliated Provincial Hospita
Cansheng Gong
gongcansheng@163.com

Fuzhou University Affiliated Provincial Hospita

Research Article

Keywords: Postoperative cognitive dysfunction, Lipocalin-2, Toll-like receptor 3, Microglial polarization, Iron-ROS pathway, Pyroptosis

Posted Date: October 1st, 2026

DOI: https://doi.org/10.21203/rs.3.rs-11022304/v1

License: This work is licensed under a Creative Commons Attribution 4.0 International License.
Read Full License

Additional Declarations: No competing interests reported.

TLR3-LCN2 Mediates Microglial M1 Polarization via Iron-ROS Signaling Pathways in Postoperative Cognitive Dysfunction

Xiangyan Jin MS[a#], Peng Ye MD[ab#], Jingwen Yu MS[a#], Ming Li PhD[c], Yongxin Huang MD[a], Ting Zheng MD[a], Zhibin Huang MD[a], Xin Zhang MD[d*], Xiaochun Zheng MD[ab*] and Cansheng Gong MD[ab*]

[a]Department of Anesthesiology, Shengli Clinical Medical College of Fujian Medical University, Fujian Provincial Hospital, Fuzhou University Affiliated Provincial Hospital, Fuzhou, Fujian, China

[b]Fujian Provincial Key Laboratory of Emergency Medicine, Fujian Provincial Key Laboratory of Critical Care Medicine, Fujian Provincial Co-Constructed Laboratory of "Belt and Road," Fujian Emergency Medical Center, Fuzhou, China

[c]Department of Anesthesiology, the Affiliated Hospital of North Sichuan Medical College, Nanchong, China.

[d]Department of Radiology, Second Affiliated Hospital of Naval Medical University, Shanghai 200003, China.

[#]Contributed equally to this work

[*]**Corresponding Author**

Cansheng Gong, MD

Phone number: +86 15859088967

E-mail: gongcansheng@163.com

Department of Anesthesiology, Shengli Clinical Medical College of Fujian Medical University, Fujian Provincial Hospital, Fuzhou University Affiliated Provincial Hospital, Fuzhou, Fujian, China,350001.

Abstract

Background: Postoperative cognitive dysfunction (POCD) is a debilitating neurological complication in elderly patients, with neuroinflammation driven by microglial activation playing a central role. Lipocalin-2 (LCN2), an iron-binding protein, is involved in various CNS pathologies, yet its specific role and upstream regulation in POCD remain poorly understood.

Methods: Aged C57BL/6J mice underwent unilateral nephrectomy to establish the POCD model. Adeno-associated virus (AAV)-mediated LCN2 knockdown was employed to evaluate its therapeutic potential. Cognitive function was assessed via the novel object recognition (NOR) and Y-maze tests. In vitro, BV2 microglia and HT-22 neurons were used to dissect the TLR3-LCN2 signaling cascade using the TLR3 agonist Poly(I:C), the iron chelator deferoxamine (DFO), and LCN2 inhibitors.

Results: Surgical stress significantly induced cognitive impairment, accompanied by upregulated TLR3 and LCN2 expression and a shift toward pro-inflammatory M1 microglial polarization in the hippocampus. Genetic knockdown of LCN2 markedly attenuated M1 polarization, reduced neuronal pyroptosis, and rescued cognitive deficits in aged mice. Mechanistically, TLR3 activation triggered LCN2 expression, which subsequently facilitated intracellular iron accumulation and reactive oxygen species (ROS) production, driving M1 polarization. Furthermore, pharmacological inhibition of the iron-ROS pathway by DFO effectively suppressed LCN2-induced M1 polarization. Microglia-neuron co-culture assays confirmed that M1-polarized microglia promoted GSDMD-dependent neuronal pyroptosis.

Conclusion: Our findings demonstrate that the TLR3-LCN2 axis exacerbates POCD by driving iron-ROS-mediated microglial M1 polarization and subsequent neuronal pyroptosis. Targeting LCN2 or the iron-ROS pathway offers a promising immunopharmacological strategy for alleviating postoperative neurocognitive impairment.

Keywords: Postoperative cognitive dysfunction; Lipocalin-2; Toll-like receptor 3; Microglial polarization; Iron-ROS pathway; Pyroptosis

Introduction

Postoperative cognitive dysfunction (POCD) is a prevalent and debilitating neurological complication characterized by impairments in memory, attention, and executive function, primarily observed in elderly patients following major surgical procedures [1]. Despite significant strides in perioperative medicine, the precise molecular underpinnings of POCD remain partially elucidated. Mounting evidence suggests that neuroinflammation, particularly the aberrant activation of microglial cells, serves as a cornerstone in the pathogenesis of POCD [2]. As the primary resident immune cells in the central nervous system (CNS), microglia act as critical sensors and effectors of physiological stress. Recent studies have demonstrated that the transition of microglia from a homeostatic state to a pro-inflammatory M1 phenotype significantly contributes to the progression of postoperative neurocognitive impairment [3].

Lipocalin-2 (LCN2), a multifaceted secretory glycoprotein originally identified for its role in innate antimicrobial defense, is expressed at minimal levels in the healthy adult brain [4, 5]. However, pathologically elevated LCN2 has been implicated in an array of CNS disorders, including ischemic stroke [5], Alzheimer's disease [6], Parkinson's disease [7], and vascular dementia [8]. Our preliminary research identified a robust upregulation of hippocampal Lcn2 mRNA in aged mice with POCD, suggesting that LCN2 may function as a pivotal mediator in the development of neurocognitive disorders [9].

Furthermore, we previously observed an increased expression of Toll-like receptor 3 (TLR3), a key pattern recognition receptor involved in sterile inflammation, within the hippocampal CA1 subfield of POCD models. Notably, genetic ablation of TLR3 was found to attenuate hippocampal neuroinflammation and improve cognitive performance [10]. Although individual roles for TLR3 and LCN2 have been proposed, the potential interaction between the TLR3 signaling pathway and LCN2 expression in the context of POCD remains elusive.

In the present study, we hypothesized that surgical stress-induced TLR3 activation triggers LCN2 secretion, which in turn orchestrates microglial M1 polarization and subsequent neuronal injury. Mechanistically, we demonstrate that the TLR3-LCN2 axis facilitates intracellular iron accumulation and the generation of reactive oxygen species (ROS), ultimately driving GSDMD-dependent neuronal pyroptosis and cognitive decline. These findings underscore the potential of LCN2 as a novel immunopharmacological target for alleviating POCD in the elderly population.

Materials and Methods

1.1 Animals and Experimental Design

Male C57BL/6J mice, aged 18-20 months, were procured from the Wushi Experimental Animal Co., Ltd. (Fuzhou, China; License No.SYXK (Min) 2018-0009). All mice were housed in a standard animal facility under controlled conditions: a 12h light/dark cycle, ambient temperature maintained at 20-24°C, 50–60% humidity, with ad libitum access to food and water. The experimental protocols adhered strictly to the National Institute of Health guidelines for the care and use of laboratory animals and were meticulously reviewed and approved by the Experimental Animal Ethics Committee of Fuzhou University Affiliated Provincial Hospital（IACUC-FPH-PZ-20241230[053]). Clinical trial number: not applicable.

1.2 Postoperative Cognitive Dysfunction (POCD) Model Establishment

The POCD model was established through a unilateral nephrectomy procedure, as previously described [11]. Briefly, mice were anesthetized with 3% isoflurane. A midline left abdominal incision was performed, followed by a standardized 10-minute abdominal exploration. Subsequently, the left kidney was carefully resected. The abdominal incision was then closed using sutures, and 0.5% ropivacaine was administered locally for postoperative analgesia. Body temperature was precisely maintained at 37 ± 0.5 °C throughout the surgical procedure using a heating pad. Post-surgery, mice received supplemental oxygen until full recovery, indicated by the return of the righting reflex. Sham-operated control mice underwent identical anesthetic

exposure, skin incision, and suturing, but without abdominal exploration or nephrectomy.

1.3 Behavioral Assessments

1.3.1 Novel Object Recognition Test (NORT)

The NORT was conducted in three distinct phases to assess non-spatial learning and memory, following established protocols [12, 13].

Habituation Phase: Each mouse was placed in the experimental chamber for 10 minutes daily for three consecutive days to acclimate to the environment.

Familiarization Phase: Two identical objects (A1 and A2) were symmetrically positioned 5 cm from the walls of the chamber. Each mouse was allowed to explore these objects for 10 minutes, and the total exploration time for A1 (TA1) and A2 (TA2) was recorded.

Discrimination Phase: One hour post-familiarization, one familiar object (A2) was replaced with a novel object (B). Mice were allowed to explore freely for 10 minutes, and exploration times for the familiar (TA1) and novel (TB) objects were recorded. The Discrimination Index (DI) was calculated as $DI = TB / (TA1 + TB) \times 100\%$. To prevent olfactory cues, the apparatus and objects were thoroughly cleaned with 70% ethanol between trials.

1.3.2 Y-maze Test

The Y-maze test was performed to evaluate spatial learning and working memory. The apparatus consisted of three identical white opaque plexiglass arms.

Training Phase: One arm (designated as the novel arm for the subsequent test) was blocked. Mice were placed at the end of an open arm (start arm) and allowed to explore the two accessible arms for 10 minutes.

Test Phase: One hour after the training phase, the mouse was returned to the start arm with all three arms accessible, including the previously blocked novel arm. The session lasted 5 minutes. The time spent in and the number of entries into each arm were

recorded and analyzed using EthoVision XT automated video tracking software (Noldus, Wageningen, Netherlands).

1.4 Immunofluorescence Staining

Following deep anesthesia, mice were transcardially perfused with ice-cold phosphate-buffered saline (PBS) followed by 4% paraformaldehyde (PFA). Brains were harvested and post-fixed in 4% PFA overnight at 4°C, then transferred to 30% sucrose solution for cryoprotection for a minimum of 72 hours. Coronal sections (20-μm-thick) were prepared using a cryostat. Sections were blocked with 3% bovine serum albumin (BSA) in PBS for 1 hour at room temperature, then incubated overnight at 4°C with the following primary antibodies: β-actin (1:200, Abcam, ab6276), LCN2 (1:50, ABclonal, A2092), TLR3 (1:50, ABclonal, A24885), NLRP3 (1:50, Proteintech, 30109-1-AP), ASC (1:50, Santa Cruz Biotechnology, sc-22514-R), Caspase-1 (1:50, Proteintech, 22915-1-AP), GSDMD (1:50, Proteintech, 20770-1-AP), IL-1β (1:50, ABclonal, A19635), IL-18 (1:50, Proteintech, 10663-1-AP), NeuN (1:50, Proteintech, 26975-1-AP), ionized calcium-binding adapter molecule 1 (Iba-1) (1:50, Proteintech, 10904-1-AP), iNOS (1:50, Proteintech, 18985-1-AP), and arginase 1 (Arg-1) (1:50, Proteintech, 66129-1-IG).

After washing thrice with PBS, sections were incubated for 1 hour at room temperature with species-appropriate secondary antibodies (goat anti-rabbit IgG, 1:200, Abcam, ab150078; goat anti-mouse IgG, 1:200, Abcam, ab150113). Fluorescence images were captured using a confocal microscope (Fluoview 1000, Olympus, Tokyo, Japan). Quantification of fluorescent-positive cells and fluorescence intensity was performed using ImageJ software.

1.5 Western Blot Analysis

Hippocampal tissues were rapidly dissected on ice and homogenized in Radioimmunoprecipitation Assay (RIPA) lysis buffer supplemented with a protease and phosphatase inhibitor cocktail (100:1, Solarbio). Lysates were centrifuged at 12,000 rpm for 20 minutes at 4°C, and the supernatants containing total protein were

collected. Protein concentrations were determined using a bicinchoninic acid (BCA) protein assay kit. Equal amounts of protein were resolved by SDS-PAGE and subsequently transferred to polyvinylidene difluoride (PVDF) membranes. Membranes were blocked for 1.5 hours at room temperature with 5% non-fat milk in Tris-buffered saline with Tween 20 (TBST).

Membranes were then incubated overnight at 4°C with the following primary antibodies: β-actin (1:2000, Abcam, ab6276), LCN2 (1:500, ABclonal, A2092), TLR3 (1:1000, ABclonal, A24885), NLRP3 (1:500, Proteintech, 30109-1-AP), ASC (1:1000, Santa Cruz Biotechnology, sc-22514-R), Caspase-1 (1:500, Proteintech, 22915-1-AP), GSDMD (1:1000, Proteintech, 20770-1-AP), IL-1β (1:500, ABclonal, A19635), and IL-18 (1:500, Proteintech, 10663-1-AP). Following three washes with TBST, membranes were incubated with horseradish peroxidase-conjugated secondary antibodies (goat anti-rabbit IgG, 1:100,000, Bioworld, BS13278; goat anti-mouse IgG, 1:100,000, Bioworld, BS12478) for 1 hour at room temperature. Target proteins were detected using an enhanced chemiluminescence (ECL) substrate and imaged with a GE Amersham Imager 600. Relative protein band intensity was quantified using ImageJ software.

1.6 Transmission Electron Microscopy (TEM)

After transcardial perfusion with 4% PFA, hippocampal tissues were meticulously dissected and post-fixed in 2.5% glutaraldehyde. Samples were then dehydrated through a graded series of ethanol and embedded in epoxy resin. Ultrathin sections were cut from the resin blocks, stained with uranyl acetate and lead citrate, and examined under a transmission electron microscope (TEM, JEM-2100, JEOL, Tokyo, Japan) to observe hippocampal ultrastructural integrity.

1.7 Stereotaxic Intracerebral Injection of AAV

Mice were anesthetized with 2% isoflurane and positioned in a stereotaxic apparatus (Narishige, Tokyo, Japan). A midline scalp incision was made to expose the skull for precise coordinate identification. A small burr hole was drilled using a dental drill. A

Hamilton syringe was used to bilaterally inject 0.2 μl of adeno-associated virus (AAV) suspension (titer: 1×10^{8} viral particles) into the hippocampal CA1 region at a constant rate of 0.05 μl/min. According to previous research [14], the stereotaxic coordinates were: anterior-posterior (AP): -2.5 mm, mediolateral (ML): ±2.0 mm, dorsoventral (DV): -1.8 mm. After injection, the needle was retained in situ for 10 minutes to facilitate viral diffusion before slow withdrawal. The burr hole was sealed with bone wax, and the incision was sutured and disinfected.

LCN2 knockdown efficiency was verified three weeks post-injection by measuring hippocampal *Lcn2* mRNA and protein expression. Viral infection efficacy was further confirmed by detecting enhanced green fluorescent protein (eGFP) expression localization via fluorescence microscopy. The AAV vectors utilized were: LCN2-AAV (HBAAV2/9-m-LCN2shRNA1-EGFP, 1.3×10^{12}vg/mL) and Control-AAV (HBAAV2/9-EGFP negative control, 1.8×10^{12} vg/mL), both purchased from Shanghai Hanheng Biotechnology Co., Ltd

1.8 Quantitative Real-time Reverse Transcription Polymerase Chain Reaction (RT-qPCR)

Total RNA was extracted from hippocampal tissue samples using the RNA Easy Fast Tissue/Cell Kit (DP451, Tiangen Biotech, China) according to the manufacturer's instructions. cDNA synthesis was performed using the PrimeScript RT PreMix Kit (RR036, Takara, Japan). Quantitative real-time PCR (RT-qPCR) was carried out using SYBR Premix Ex Taq (RR820, Takara) on a Bio-Rad CFX Connect Real-Time PCR Detection System. The following specific primers were used to amplify the target sequence for LCN2:

Forward: 5'-GCTGACTTCGGAACTAAAGGAGAA-3'

Reverse: 5'-GGGAAGACGATGTGGTTTTCA-3'

1.9 Cell Culture

The BV2 microglial cell line (ATCC No. CRL-1834) was obtained from Shanghai

Fuheng Biotechnology Co., Ltd. The HT-22 neuronal cell line was acquired from the Institute of Basic Medical Sciences, Chinese Academy of Sciences. Both cell lines were maintained in high-glucose Dulbecco's Modified Eagle Medium (DMEM) supplemented with 10% fetal bovine serum (FBS) and 1% penicillin/streptomycin in a humidified atmosphere of 5% CO2 at 37°C.

1.10 Microglia-Neuron Co-culture System

A Transwell chamber system was utilized to establish the microglia-neuron co-culture model. HT-22 neuronal cells were initially seeded in the lower chamber at densities of 5×10^4 cells/well (6-well plate) or 2×10^4 cells/well (24-well plate). After 24 hours of incubation to allow for adherence and initial growth, BV2 microglial cells were seeded in the upper chamber inserts at densities of 5×10^4 cells/well (6-well) or 1×10^4 cells/well (24-well) to facilitate 48-hour paracrine interaction.

The study comprised two main groups: a co-culture group and an HT-22-only group. Each major group was further subdivided into four treatment groups: control (untreated), lipopolysaccharide (LPS)-treated (100 ng/ml for 24h), Poly(I:C)-treated (100 μg/ml for 24h), and IL-4-treated (20 ng/ml for 24h). Following treatment, Transwell inserts were removed. Neuronal cells in the lower chamber were then processed for immunofluorescence staining or collected as cell lysates for Western blot analysis of target proteins.

1.11 Flow Cytometry for Intracellular Reactive Oxygen Species (ROS) Detection

Microglial cells (BV2) were seeded at a density of 3×10^5 cells per well in 6-well plates and allowed to adhere for 24 hours. Cells were then treated with: normal culture medium (control), 100 μg/ml Poly(I:C) for 24h, 1 μg/ml recombinant LCN2 (rLCN2) for 12h, or 1 μM deferoxamine (DFO) for 12h. Post-treatment, supernatants were discarded, and cells were washed three times with serum-free DMEM. Cells were then incubated with a 1:1000 dilution of DCFH-DA (or equivalent ROS probe, e.g., DCF, Invitrogen, Cat# D399) in serum-free medium at 37°C for 30 minutes in the dark. After removing the probe solution, cells were trypsinized, collected, and resuspended in 1 ml

PBS for flow cytometry analysis (excitation/emission: 488/525 nm) using a BD FACSCalibur flow cytometer. Data were processed using FlowJo software (version X.0).

1.12 Intracellular Divalent Iron (Fe2+) Detection

Microglial cells (BV2) were seeded in fluorescence-compatible culture dishes and incubated overnight at 37°C with 5% CO2. After removing the supernatant, cells were washed three times with Hanks' Balanced Salt Solution (HBSS) and treated for 24h with 100 μg/ml Poly(I:C), or for 12h with either 1 μg/ml rLCN2 or 1 μM DFO in fresh medium. Following treatment, the medium was replaced with 1 μmol/L FerroOrange working solution (Dojindo Molecular Technologies, Inc., Cat# F374) and incubated for 30 minutes at 37°C. Cellular fluorescence, indicative of intracellular Fe2+ levels, was immediately visualized and imaged using an inverted fluorescence microscope (Ex/Em: 543/580 nm). Quantification of fluorescence intensity was performed using ImageJ software.

1.13 Statistical Analysis

All graphical representations and statistical analyses were performed using GraphPad Prism 9.0 (GraphPad Software Inc., CA, USA). Data are presented as the mean ± standard error of the mean (SEM). Differences between two independent groups were analyzed by unpaired two-tailed Student's t-test. For multiple group comparisons, one-way ANOVA followed by Bonferroni post hoc test was used. No data points were excluded from the statistical analysis. A p-value < 0.05 was considered statistically significant.

2. Results

2.1 Surgical Stress Triggers Cognitive Impairment in Aged Mice

To evaluate the impact of surgical stress on cognitive function, we performed the Novel Object Recognition Test (NORT) and Y-maze test (**Fig. 1A-B**). In the NORT, behavioral trajectory analysis revealed that mice in the surgery group exhibited significantly less complex exploration patterns toward novel objects compared to the sham group (**Fig. 1C**). Quantitative analysis confirmed a substantial reduction in the Discrimination Index (DI) in surgical mice (**Fig. 1F**), indicating impaired recognition memory. Consistently, in the Y-maze test, the surgery group demonstrated dual deficits in spatial exploration, characterized by significantly reduced diminished distance traveled within the novel arm (**Fig. 1G**) and exploration time (**Fig. 1H**). These findings collectively demonstrate that surgical trauma induced by unilateral nephrectomy, combined with anesthesia, leads to robust impairments in both recognition and spatial memory in aged mice.

2.2 Surgical Stress Upregulates the TLR3-LCN2 Axis and Promotes M1 Polarization and Neuronal Pyroptosis

We next investigated the molecular changes in the hippocampus following surgery. Western blot analysis showed a significant elevation in LCN2 protein levels within the hippocampal CA1 subregion of surgical mice compared to sham controls (**Fig. 2A, B**). Dual immunofluorescence staining for LCN2 and the microglial marker IBA-1 revealed a pronounced increase in LCN2+/IBA-1+ co-localized cells, suggesting that activated microglia are a primary source of LCN2 post-surgery (**Fig. 2C, D**). Building on our previous findings [15], we observed a concomitant upregulation of TLR3 protein (**Fig. 2E, F**) and its increased co-localization with IBA-1+ microglia in the CA1 region (**Fig. 2G, H**).

Regarding microglial polarization, surgery induced a marked increase in the M1 marker iNOS and a significant decrease in the M2 marker Arg1 (**Fig. 3A, C**), indicating a pro-inflammatory phenotypic shift. This was further corroborated by increased levels of compensatory anti-inflammatory response cytokines (IL-10 and others) (**Fig. 3B, D**).

Furthermore, key proteins of the pyroptosis pathway, including NLRP3, GSDMD, caspase-1, ASC, IL-18, and IL-1β, were significantly upregulated in the surgical group (**Fig. 3E, F**). Transmission electron microscopy (TEM) provided ultrastructural evidence of neuronal injury, showing plasma membrane rupture and perinuclear vacuolization in the surgery group (**Fig. 3G**). Notably, GSDMD immunoreactivity was predominantly localized in NeuN+ neurons rather than IBA-1+ microglia (**Fig. 3H, I**), suggesting that M1-polarized microglia primarily drive neuronal pyroptosis in this model.

2.3 AAV-Mediated LCN2 Knockdown Attenuates Microglial M1 Polarization and Neuroinflammation

To determine the functional necessity of LCN2, we employed AAV-mediated shRNA to knockdown LCN2 in the hippocampus (**Fig. 4A-B**). Successful knockdown was validated by a significant reduction in *Lcn2* mRNA levels (**Fig.4C**). Immunofluorescence analysis demonstrated that LCN2 knockdown effectively suppressed the surgery-induced increase in iNOS+ cells while facilitating an increase in Arg1+ cells (**Fig. 4D-E**). Additionally, the surgical group's elevated levels of pro-inflammatory factors (IL-6, IL-1β) were significantly mitigated by LCN2 knockdown (**Fig. 4F-G**). Western blot analysis further confirmed that LCN2 deficiency reduced the expression of pyroptosis-related proteins triggered by surgery (**Fig.4H-I**). Correspondingly, the number of GSDMD-positive neurons was significantly lower in the shLCN2+surgery group compared to the shControl+surgery group (**Fig. 4J-K**), and TEM revealed improved membrane integrity in hippocampal neurons (**Fig. 4L**).

2.4 LCN2 Deficiency Rescues Postoperative Cognitive Deficits

Following the observation of reduced neuroinflammation, we assessed whether LCN2 knockdown could rescue cognitive function. In the NORT, mice in the shLCN2+surgery group showed a significantly higher novel object recognition index compared to the shControl+surgery group (**Fig. 5A-B**). Similarly, in the Y-maze test, LCN2 knockdown substantially increased the exploration time and distance in the novel arm relative to the surgery-only group (**Fig. 5C-D**). These results indicate that targeting LCN2 is a viable strategy to alleviate surgery-induced cognitive impairment.

2.5 LCN2 Orchestrates M1 Polarization via Iron Accumulation and ROS Generation In Vitro

As an iron-binding protein, we hypothesized that LCN2 modulates polarization through iron-dependent mechanisms [16]. In primary microglial cultures, recombinant LCN2 (rLCN2) treatment significantly increased the proportion of iNOS+ M1 cells (**Fig. 6B-C**). This effect was largely abrogated by co-treatment with the iron chelator deferoxamine (DFO). Furthermore, flow cytometry and fluorescence staining revealed that rLCN2 treatment markedly elevated intracellular reactive oxygen species (ROS) and ferrous iron (Fe^{2+}) levels, both of which were effectively suppressed by DFO (**Fig. 6D-G**). These data suggest that LCN2 drives microglial M1 polarization by facilitating iron overload and subsequent ROS accumulation.

2.6 TLR3 Activation Acts as an Upstream Trigger for LCN2-Induced Microglial Polarization

To elucidate the upstream regulation of LCN2, BV2 microglial cells were treated with the TLR3 agonist Poly(I:C) [17]. TLR3 activation led to a significant increase in LCN2 protein expression and fluorescence intensity (**Fig. 7B-E**). Concurrently, Poly(I:C) treatment promoted M1 polarization (increased iNOS) and inhibited the M2 phenotype (decreased Arg1) (**Fig.7F,G**). Crucially, co-treatment with an LCN2 inhibitor (ZINC00640089) significantly attenuated the Poly(I:C)-induced M1 shift (**Fig. 7F, G**), which was accompanied by reduced intracellular ROS production and iron accumulation (**Fig. 7H-K**)

2.7 M1-Polarized Microglia Drive Neuronal Pyroptosis via the TLR3-LCN2 Axis

Surgical stress was observed to promote microglial M1 polarization and neuronal pyroptosis in vivo; however, the causal relationship between these processes remains unclear. Previous studies in oxygen-glucose deprivation/reoxygenation (OGD/R) models demonstrated that LPS-induced microglial M1 polarization exacerbates neuronal pyroptosis, whereas IL-4-induced M2 polarization suppresses it [18]. Nevertheless, whether microglial M1 polarization directly drives neuronal pyroptosis in postoperative cognitive dysfunction (POCD) models requires further investigation.

Finally, using a microglia-neuron co-culture system, we assessed the causal link between microglial polarization and neuronal death (**Fig. 8A**). Microglia treated with LPS or Poly(I:C) (M1-polarized) significantly upregulated the pyroptosis executioner protein GSDMD in HT-22 neurons (**Fig. 8B-C**). In contrast, IL-4-induced M2 microglia did not increase neuronal GSDMD levels and even conferred a protective effect against baseline injury (**Fig. 8D**). Immunofluorescence confirmed a marked increase in GSDMD intensity in neurons co-cultured with M1-polarized microglia. Collectively, these results indicate that the TLR3-LCN2 signaling pathway promotes neuronal pyroptosis by inducing a pro-inflammatory microglial phenotype.

Discussion

In this study, we examined the specific effects of Lipocalin-2 on cognitive function and elucidated its upstream and downstream mechanisms in the context of postoperative cognitive dysfunction. Our findings indicate that LCN2 exacerbates cognitive impairment by facilitating microglial M1 polarization and subsequent neuronal pyroptosis. Additionally, we identified Toll-like receptor 3 as the upstream regulator of LCN2-induced microglial M1 polarization and uncovered a downstream mechanism involving the iron-reactive oxygen species pathway.

Previous research conducted by our team demonstrated an 8.18-fold increase in LCN2 mRNA expression within the hippocampal CA1 region of mice subjected to unilateral nephrectomy, which was associated with postoperative cognitive decline [9]. The present study further corroborated these findings by employing Western blot and immunofluorescence assays, which revealed that surgical-anesthetic stress significantly elevates LCN2 protein expression in the hippocampal microglia of aged mice. Subsequent experiments indicated that LCN2 knockdown substantially ameliorated postoperative cognitive function in aged mice, thereby establishing its pivotal role in the pathogenesis of postoperative cognitive dysfunction. In alignment with our results, previous studies on POCD models have reported significant associations between hippocampal LCN2 levels, microglial activation, and impairments in exploratory behavior and spatial learning, as assessed by Morris water maze tests [19]. Importantly, this research definitively identified LCN2 as an upstream regulator of microglial M1

polarization and neuronal pyroptosis in POCD. Notably, even under conditions of microglial depletion, LCN2 expression remained significantly elevated in the brains of POCD model mice, suggesting the presence of non-microglial sources of LCN2 [14]. Nevertheless, the depletion of microglia significantly enhanced cognitive function, underscoring the essential role of microglia-mediated pathophysiological processes in cognitive impairment induced by surgical procedures. Furthermore, our findings revealed that the knockdown of Lipocalin-2 (LCN2) influences the polarization of microglia towards the M1 phenotype, mitigates neuroinflammation and neuronal pyroptosis, and consequently improves postoperative cognitive recovery in murine models.

The neuroinflammatory microenvironment in the hippocampus following surgical stress is a complex milieu characterized by the dynamic interplay between various CNS resident cells [20]. Our findings suggest that POCD is not merely a localized immune response, but a synchronized cascade where LCN2 acts as a crucial orchestrator. Although LCN2 expression remained detectable after microglial depletion, its primary pathological impact in our model was the facilitation of a pro-inflammatory M1-like phenotype shift in the remaining or repopulated microglia. This LCN2-driven polarization creates a self-amplifying loop of oxidative stress and inflammatory cytokine release, which ultimately compromises neuronal integrity. Therefore, identifying the precise molecular triggers that initiate LCN2 upregulation within this neuroinflammatory niche is of paramount importance for therapeutic intervention.

Previous studies have demonstrated that TLR3 facilitates increased LCN2 expression in small intestinal epithelial cells [17], with TLR3 knockdown significantly reducing LCN2 levels, thereby first elucidating their interaction. However, such a relationship had not been previously identified within the central nervous system. Our research has identified that TLR3 augments LCN2 expression in microglia, thereby establishing their interaction in CNS cells for the first time. TLR3 is known to play critical roles in the CNS, as prior research has shown that heightened TLR3 signaling exacerbates postoperative cognitive deficits and cognitive decline associated with chronic neuropathic pain [15, 21], while TLR3 deficiency mitigates sevoflurane-induced

programmed necrosis in neonatal mice [10]. Nevertheless, these studies did not successfully clarify the precise signaling mechanisms associated with TLR3. Our research demonstrates that TLR3 induces the upregulation of LCN2, which promotes microglial M1 polarization through the iron-ROS pathway, ultimately leading to neuronal pyroptosis. This elucidates a novel TLR3-LCN2-iron/ROS regulatory axis involved in neuroinflammation and cognitive impairment.

Studies [22] have found that LCN2 is highly expressed in glutamate-induced HT22 cell models, and LCN2 knockdown significantly reduces Fe^{2+} levels and inhibits iron accumulation. Another study demonstrated that under Fe^{2+} overload conditions [23], treatment with LCN2 siRNA or LCN2 R siRNA did not reduce Fe^{2+} uptake in H9c2 cardiomyocytes, whereas under Fe^{3+} overload conditions, treatment with LCN2 siRNA, LCN2 R siRNA, and DFP significantly decreased Fe^{3+} uptake in H9c2 cardiomyocytes, further indicating that LCN2 directly regulates intracellular Fe^{2+} levels, iron uptake, and iron accumulation. Additional research[16] revealed that Fe^{2+} content and lipid ROS levels were markedly reduced in LCN2-knockdown cell lines (HT29-SHB/shLCN2), while both lipid ROS levels and intracellular Fe^{2+} content were upregulated in LCN2-overexpressing cells (SW620-OB/OVER-LCN2), providing evidence for the interaction between LCN2 and the iron-ROS pathway. Our study also confirmed that LCN2 promotes increased Fe^{2+} content and elevated ROS levels in microglia, further supporting the interplay between LCN2 and the iron-ROS regulatory axis.

Pyroptosis, a form of programmed cell death characterized by inflammasome activation, Caspase-1 cleavage, and the release of pro-inflammatory cytokines, has been demonstrated to closely correlate with cognitive dysfunction when occurring in astrocytes, microglia, or neurons[24-26] . This correlation provides novel insights into the pathological mechanisms underlying cognitive impairment. The present study observed that surgical-anesthetic stress led to a significant increase in GSDMD expression in hippocampal neurons, which was accompanied by cytoplasmic shrinkage, plasma membrane rupture, and peripheral multivesiculation, indicative of neuronal pyroptosis. In contrast, microglial pyroptosis was not prominently observed, aligning with the findings of Wei et al. [27, 28]. However, other studies have reported that

pyroptosis in microglia or astrocytes contributes to the development of postoperative cognitive dysfunction [24-26], suggesting that the occurrence of cell-type-specific pyroptosis may vary depending on the experimental models and conditions employed. However, our study has several limitations. First, although the AAV-mediated LCN2 knockdown achieved targeted intervention in the hippocampal region, it lacked cell type-specific knockdown, preventing us from distinguishing the specific roles of LCN2 in different cell types. Future studies should design more precise AAV vectors to investigate cell-specific mechanisms in POCD. Second, while the BV2 cell line is widely used in microglial research, potential genetic and functional differences between this cell line and in vivo microglia exist, necessitating further validation using primary microglia or in vivo experiments. Third, the co-culture system employed partially mimics microglia-neuron interactions but remains physiologically distant from the complex in vivo microenvironment; future studies could utilize 3D cultures or organoid models to enhance physiological relevance. Fourth, in vitro experiments utilized recombinant LCN2 protein, TLR3 agonists, and the LCN2 inhibitor ZINC to modulate microglia, rather than directly manipulating TLR3 expression through overexpression or knockdown via viral transduction, which may affect the rigor of mechanistic validation for TLR3-LCN2 interactions. Fifth, while we observed LCN2-mediated intracellular iron accumulation, ferroptosis—an iron-dependent, non-apoptotic cell death characterized by lipid peroxidation accumulation and antioxidant system collapse [29]—requires further investigation to determine its occurrence in microglia and neurons.

Funding Statement: This work was supported by the National Natural Science Foundation of China, Grant Number: 82471278; Natural Science Foundation of Fujian Province, Grant Number: 2021J01385; Fujian provincial health technology project, Grant Number: 2022GGA007; The special cooperation project between Nanchong city and North Sichuan Medical College, Grant Number: 22SXQT0026.

Conflicts of Interest: The authors declare no competing interests.

References

1. Evered L, Silbert B, Knopman DS, Scott DA, DeKosky ST, Rasmussen LS, Oh ES, Crosby G, Berger M, Eckenhoff RG: **Recommendations for the nomenclature of cognitive change associated with anaesthesia and surgery-2018**. *Br J Anaesth* 2018, **121**(5):1005-1012.
2. Feng X, Valdearcos M, Uchida Y, Lutrin D, Maze M, Koliwad SK: **Microglia mediate postoperative hippocampal inflammation and cognitive decline in mice**. *JCI Insight* 2017, **2**(7):e91229.
3. AmeliMojarad M, AmeliMojarad M: **The neuroinflammatory role of microglia in Alzheimer's disease and their associated therapeutic targets**. *CNS Neurosci Ther* 2024, **30**(7):e14856.
4. Nairz M, Theurl I, Schroll A, Theurl M, Fritsche G, Lindner E, Seifert M, Crouch ML, Hantke K, Akira S *et al*: **Absence of functional Hfe protects mice from invasive Salmonella enterica serovar Typhimurium infection via induction of lipocalin-2**. *Blood* 2009, **114**(17):3642-3651.
5. Li J, Xu P, Hong Y, Xie Y, Peng M, Sun R, Guo H, Zhang X, Zhu W, Wang J *et al*: **Lipocalin-2-mediated astrocyte pyroptosis promotes neuroinflammatory injury via NLRP3 inflammasome activation in cerebral ischemia/reperfusion injury**. *J Neuroinflammation* 2023, **20**(1):148.
6. Kang H, Shin HJ, An HS, Jin Z, Lee JY, Lee J, Kim KE, Jeong EA, Choi KY, McLean C *et al*: **Role of Lipocalin-2 in Amyloid-Beta Oligomer-Induced Mouse Model of Alzheimer's Disease**. *Antioxidants (Basel)* 2021, **10**(11).
7. Jiang SY, Tian T, Yao H, Xia XM, Wang C, Cao L, Hu G, Du RH, Lu M: **The cGAS-STING-YY1 axis accelerates progression of neurodegeneration in a mouse model of Parkinson's disease via LCN2-dependent astrocyte senescence**. *Cell Death Differ* 2023, **30**(10):2280-2292.
8. Li X, Wang X, Guo L, Wu K, Wang L, Rao L, Liu X, Kang C, Jiang B, Li Q *et al*: **Association between lipocalin-2 and mild cognitive impairment or dementia: A systematic review and meta-analysis of population-based evidence**. *Ageing Res Rev* 2023, **89**:101984.
9. Li M, Chen C, Zhang W, Gao R, Wang Q, Chen H, Zhang S, Mao X, Leblanc M, Behensky A *et al*: **Identification of the Potential Key Long Non-coding RNAs in Aged Mice With Postoperative Cognitive Dysfunction**. *Front Aging Neurosci* 2019, **11**:181.

10. MacDowell KS, Munarriz-Cuezva E, Caso JR, Madrigal JL, Zabala A, Meana JJ, García-Bueno B, Leza JC: **Paliperidone reverts Toll-like receptor 3 signaling pathway activation and cognitive deficits in a maternal immune activation mouse model of schizophrenia**. *Neuropharmacology* 2017, **116**:196-207.

11. Chen C, Cai J, Zhang S, Gan L, Dong Y, Zhu T, Ma G, Li T, Zhang X, Li Q *et al*: **Protective Effect of RNase on Unilateral Nephrectomy-Induced Postoperative Cognitive Dysfunction in Aged Mice**. *PLoS One* 2015, **10**(7):e0134307.

12. Lueptow LM: **Novel Object Recognition Test for the Investigation of Learning and Memory in Mice**. *J Vis Exp* 2017(126).

13. Liao YL, Zhou XY, Ji MH, Qiu LC, Chen XH, Gong CS, Lin Y, Guo YH, Yang JJ: **S100A9 Upregulation Contributes to Learning and Memory Impairments by Promoting Microglia M1 Polarization in Sepsis Survivor Mice**. *Inflammation* 2021, **44**(1):307-320.

14. Xiang X, Tang X, Yu Y, Xie S, Liu L, Chen M, Zhang R, Kang X, Zheng Y, Yang G *et al*: **Role of lipocalin-2 in surgery-induced cognitive decline in mice: a signal from neuron to microglia**. *J Neuroinflammation* 2022, **19**(1):92.

15. Chen C, Gao R, Li M, Wang Q, Chen H, Zhang S, Mao X, Behensky A, Zhang Z, Gan L *et al*: **Extracellular RNAs-TLR3 signaling contributes to cognitive decline in a mouse model of postoperative cognitive dysfunction**. *Brain Behav Immun* 2019, **80**:439-451.

16. Feng M, Wu X, Zhang J, Chen P, Qian S, Chang C: **Loss of Lipocalin2 confers cisplatin vulnerability through modulating NF-κB mediated ferroptosis via ferroportin**. *Am J Cancer Res* 2024, **14**(5):2088-2102.

17. Østvik AE, Granlund AV, Torp SH, Flatberg A, Beisvåg V, Waldum HL, Flo TH, Espevik T, Damås JK, Sandvik AK: **Expression of Toll-like receptor-3 is enhanced in active inflammatory bowel disease and mediates the excessive release of lipocalin 2**. *Clin Exp Immunol* 2013, **173**(3):502-511.

18. Dong Z, Peng Q, Pan K, Lin W, Wang Y: **Microglial and Neuronal Cell Pyroptosis Induced by Oxygen-Glucose Deprivation/Reoxygenation Aggravates Cell Injury via Activation of the Caspase-1/GSDMD Signaling Pathway**. *Neurochem Res* 2023, **48**(9):2660-2673.

19. Lou L, Yu W, Cheng Y, Lin Q, Jiang Y, Wang D, Che L, Du M, Wang S, Zhen H: **Quercetin can improve anesthesia induced neuroinflammation and cognitive dysfunction by**

regulating miR-138-5p/ LCN2. *BMC Anesthesiol* 2025, **25**(1):21.

20. Zheng Y, Xu W, Suo Z, Qu Y, Lin L, Zhang E, Han D, Wu M, Li H, Zheng H *et al*: **Inflammation associated microglial expansion disrupts hippocampal glial network communication, driving postoperative neurocognitive impairment**. *J Neuroinflammation* 2025, **22**(1):256.

21. Zhang X, Gao R, Zhang C, Teng Y, Chen H, Li Q, Liu C, Wu J, Wei L, Deng L *et al*: **Extracellular RNAs-TLR3 signaling contributes to cognitive impairment after chronic neuropathic pain in mice**. *Signal Transduct Target Ther* 2023, **8**(1):292.

22. Luo L, Deng L, Chen Y, Ding R, Li X: **Identification of Lipocalin 2 as a Ferroptosis-Related Key Gene Associated with Hypoxic-Ischemic Brain Damage via STAT3/NF-κB Signaling Pathway**. *Antioxidants (Basel)* 2023, **12**(1).

23. Kumfu S, Siri-Angkul N, Chattipakorn SC, Chattipakorn N: **Silencing of lipocalin-2 improves cardiomyocyte viability under iron overload conditions via decreasing mitochondrial dysfunction and apoptosis**. *J Cell Physiol* 2021, **236**(7):5108-5120.

24. Chen Y, Wei G, Feng X, Lei E, Zhang L: **Dexmedetomidine enhances Mitophagy via PINK1 to alleviate hippocampal neuronal Pyroptosis and improve postoperative cognitive dysfunction in elderly rat**. *Exp Neurol* 2024, **379**:114842.

25. Shen J, Xu J, Wen Y, Tang Z, Li J, Sun J: **Carnosine ameliorates postoperative cognitive dysfunction of aged rats by limiting astrocytes pyroptosis**. *Neurotherapeutics* 2024, **21**(4):e00359.

26. Wang W, Gao W, Gong P, Song W, Bu X, Hou J, Zhang L, Zhao B: **Neuronal-specific TNFAIP1 ablation attenuates postoperative cognitive dysfunction via targeting SNAP25 for K48-linked ubiquitination**. *Cell Commun Signal* 2023, **21**(1):356.

27. Wang W, Gao W, Zhang L, Xia Z, Zhao B: **SNAP25 ameliorates postoperative cognitive dysfunction by facilitating PINK1-dependent mitophagy and impeding caspase-3/GSDME-dependent pyroptosis**. *Exp Neurol* 2023, **367**:114463.

28. Zhao N, Xu X, Jiang Y, Gao J, Wang F, Xu X, Wen Z, Xie Y, Li J, Li R *et al*: **Lipocalin-2 may produce damaging effect after cerebral ischemia by inducing astrocytes classical activation**. *J Neuroinflammation* 2019, **16**(1):168.

29. Kayagaki N, Kornfeld OS, Lee BL, Stowe IB, O'Rourke K, Li Q, Sandoval W, Yan D, Kang J, Xu M *et al*: **NINJ1 mediates plasma membrane rupture during lytic cell death**. *Nature* 2021,

591(7848):131-136.

Figure legend

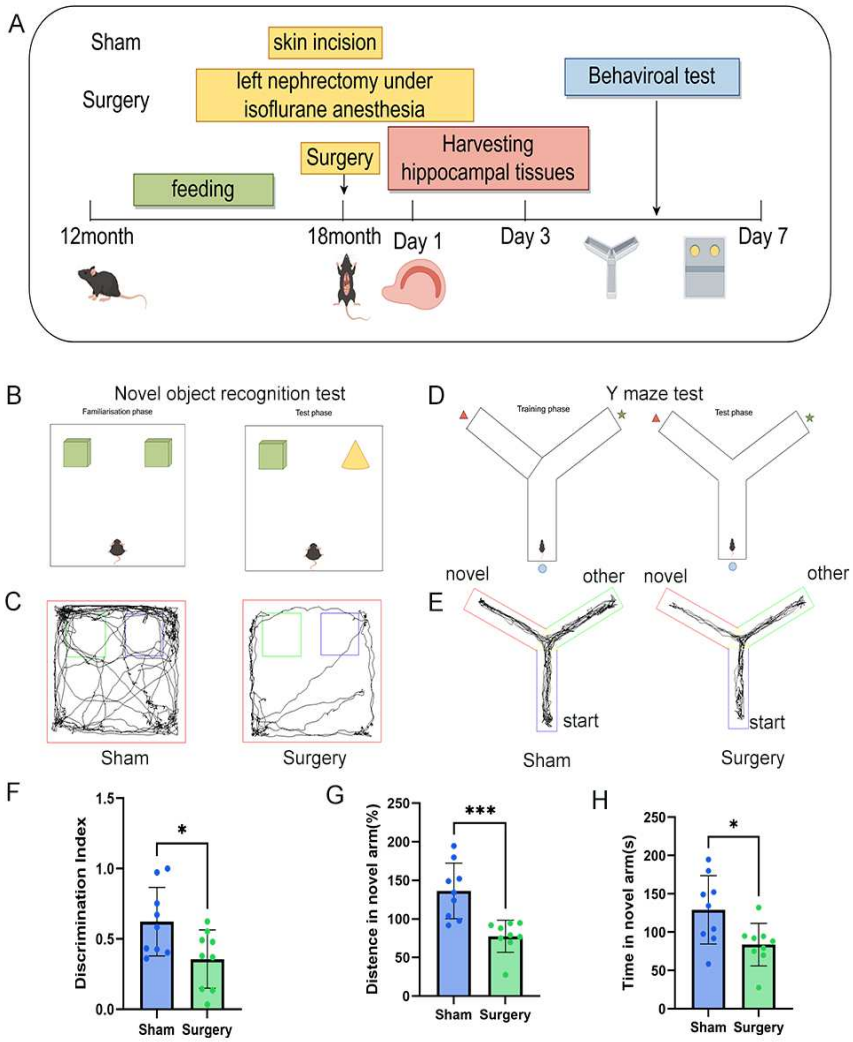


Figure 1: Postoperative cognitive impairment resulting from surgical stress in aged mice was investigated through various experimental setups. (A) A schematic diagram illustrates the experimental design. (B) The setup for the novel object recognition (NOR) test is depicted. (C) Representative outcomes from the NOR test are presented. (D) A schematic diagram details the Y-maze test setup. (E) Representative outcomes from the Y-maze test are provided. (F) A quantitative analysis of the Discrimination Index from the NOR test is shown, with data expressed as mean ± SEM; *P < 0.05, n = 9. (G, H) The quantitative analysis of spontaneous alternation behavior in the Y-maze test is presented, with data expressed as mean ± SEM; *P < 0.05, ***P < 0.001, n = 9.

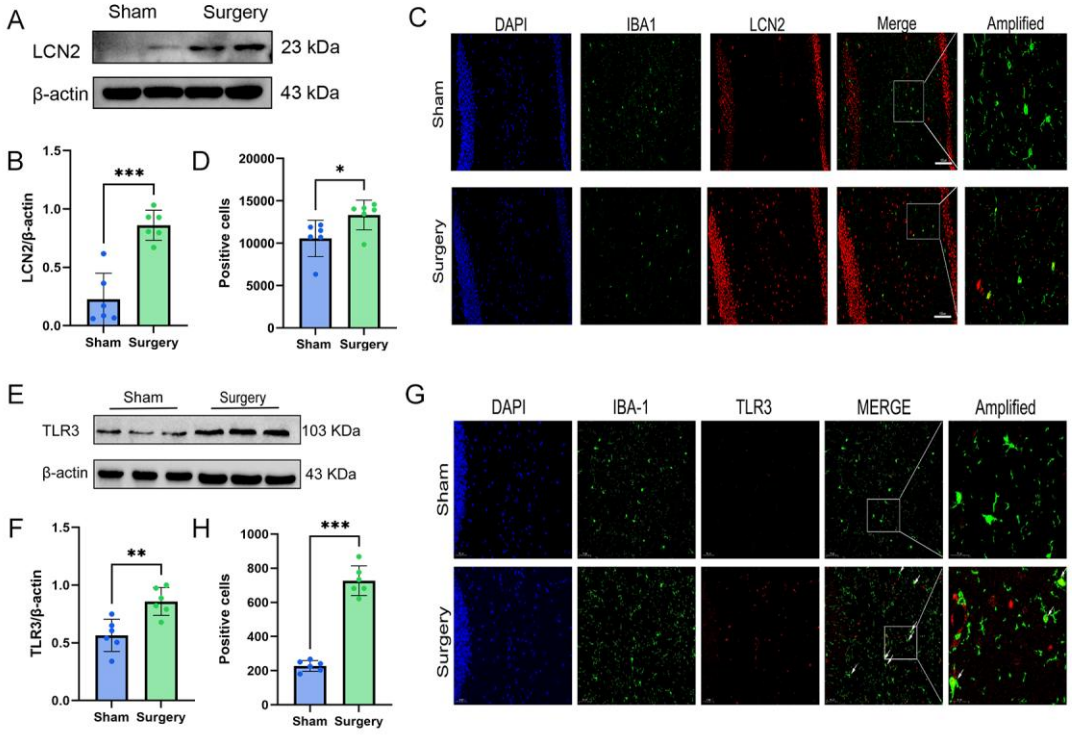


Figure 2: Surgical stress leads to an upregulation of LCN2 and TLR3 secretion. (A, B) Western blot analyses were conducted to assess LCN2 protein levels in hippocampal tissue, accompanied by corresponding quantitative data. Results are expressed as mean ± SEM; ***P < 0.001, n = 6. (C, D) Immunofluorescence co-localization studies demonstrate the presence of LCN2 (red) alongside the microglial marker IBA1 (green) within the hippocampal CA1 region. Quantitative analysis is provided in panel D. Results are expressed as mean ± SEM; *P < 0.05, n = 6. (E, F) Western blot analyses were performed to evaluate TLR3 protein levels in hippocampal tissue, with associated quantitative results. Results are expressed as mean ± SEM; **P < 0.01, n = 6. (G, H) Immunofluorescence co-localization studies reveal the presence of TLR3 (red) with the microglial marker IBA1 (green) in the hippocampal CA1 region. Quantitative analysis is provided in panel H. Results are expressed as mean ± SEM; ***P < 0.001, n = 6.

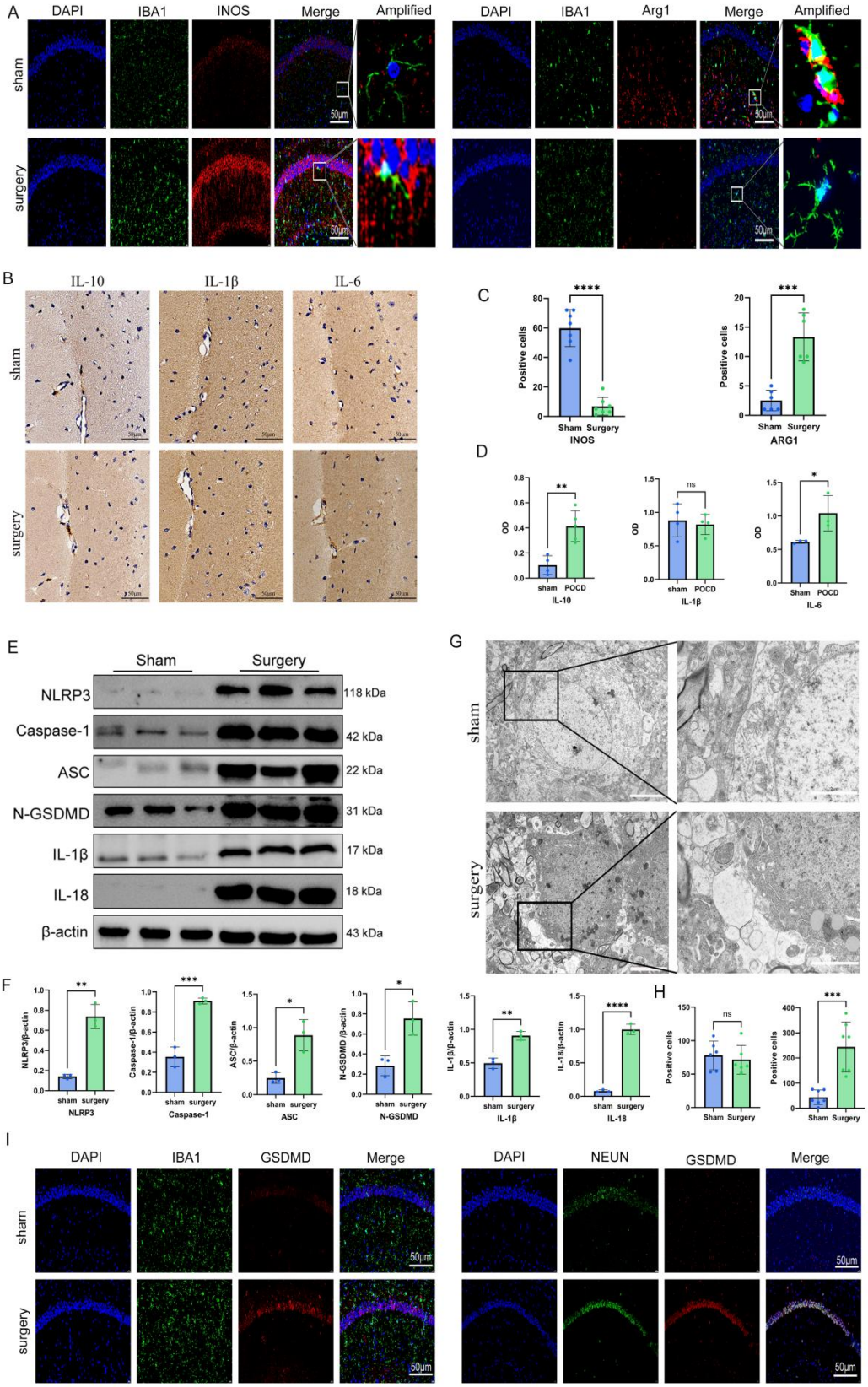


Figure 3: Surgical stress induces M1 polarization of microglia and facilitates

neuronal pyroptosis. (A) Representative immunofluorescence images illustrating the co-localization of IBA-1 with ARG1 and IBA-1 with iNOS. (B) Representative immunohistochemical images depicting the expression of IL-10, IL-1β, and IL-6 in the hippocampal CA1 region. (C) Quantitative analysis of iNOS and ARG1 immunofluorescence intensity. Data are expressed as mean ± SEM; ***P < 0.001, n = 6 to 7. (D) Quantitative analysis of IL-10, IL-1β, and IL-6 immunohistochemical staining intensity in the hippocampus. Data are expressed as mean ± SEM; **P < 0.01, ***P < 0.001, ns. not significant, n = 6. (E, F) The expression of pyroptosis-related proteins in hippocampal tissue was analyzed using Western blotting, with corresponding quantitative results provided. Data are expressed as mean ± SEM; statistical significance is indicated as *P < 0.05, **P < 0.01, ***P < 0.001, with a sample size of n = 3. (G) Transmission electron microscopy (TEM) images illustrate the hippocampal ultrastructure in both the Sham and Surgery groups. (H, I) Immunofluorescence co-localization analysis was conducted to examine the association of GSDMD with the microglial marker IBA1 (left panel) and the neuronal marker NeuN (right panel). Quantitative analysis of fluorescence intensity is presented in panel H. Data are expressed as mean ± SEM; statistical significance is denoted as **P < 0.01, ***P < 0.001, with "ns" indicating no significance, and a sample size of n = 7.

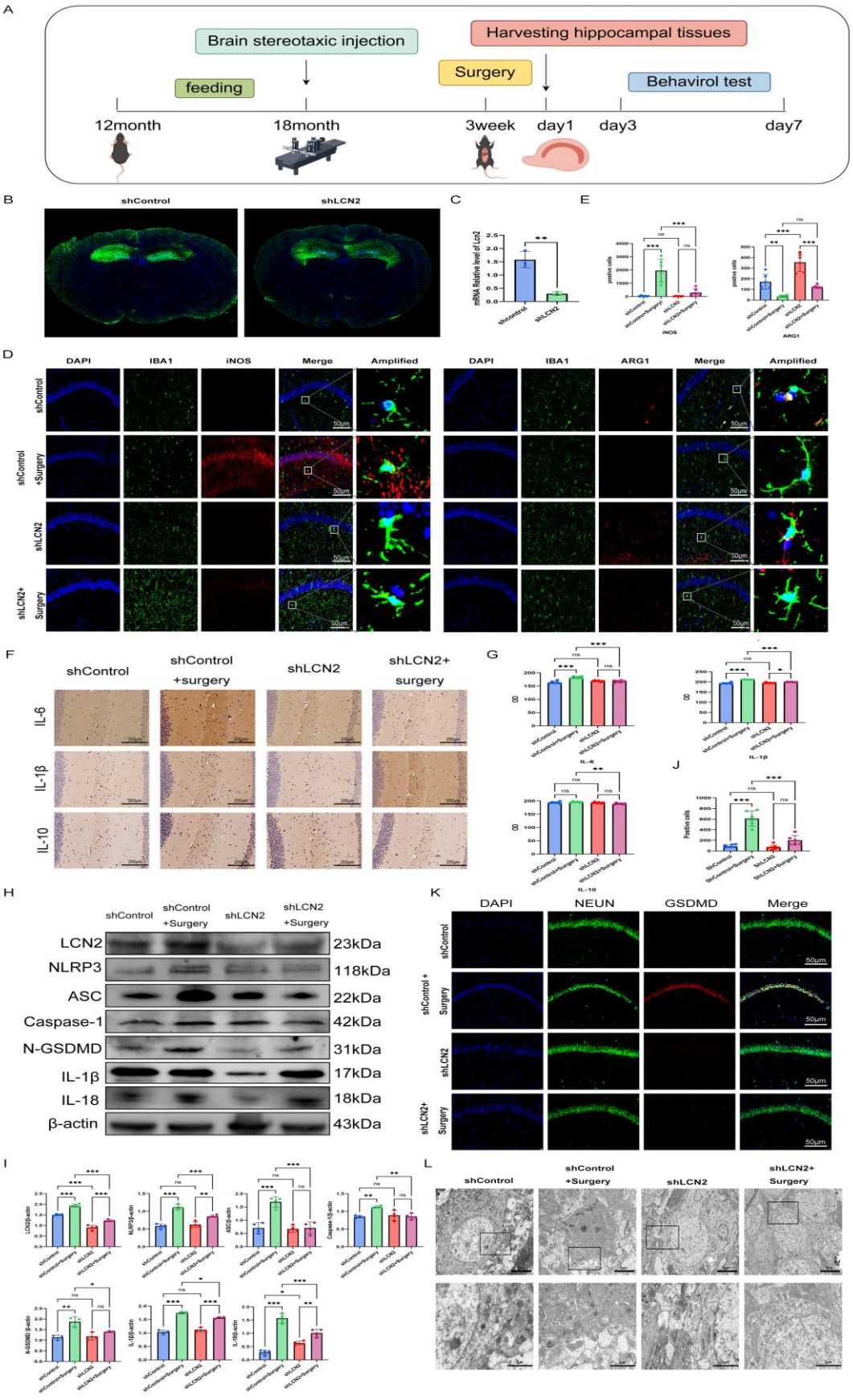


Figure 4: The Knockdown of LCN2 Mitigates Microglial M1 Polarization and Neuronal Pyroptosis. (A) Timeline illustrating the sequence of AAV injection, model

establishment, behavioral assessments, and sample collection. (B) Fluorescence microscopy images depicting the hippocampal CA1 region following the administration of control virus (shControl) and shLCN2 virus. (C) Quantitative PCR analysis of LCN2 mRNA expression levels in the hippocampus, with statistical significance denoted as **P < 0.01, n=3. (D) Representative immunofluorescence images showing ARG1, iNOS, and microglia within the hippocampal CA1 region. (E) Quantitative assessment of ARG1- and iNOS-positive cells co-localized with microglia. Data are expressed as mean ± SEM; statistical significance is indicated as *P < 0.05, **P < 0.01, ***P < 0.01, n = 6. (F) Immunohistochemical analysis was conducted to assess the expression of IL-10, IL-1β, and IL-6 within the hippocampus. (G) The expression levels of IL-10, IL-1β, and IL-6 were quantified, with statistical significance denoted as follows: *P < 0.05, **P < 0.01, ***P < 0.001, n = 6. (H) Representative Western blot images illustrate the expression of LCN2 and proteins associated with pyroptosis, including NLRP3, Caspase-1, ASC, N-GSDMD, IL-1β, and IL-18. (I) Quantitative analysis of the expression levels of LCN2 and pyroptosis-associated proteins (NLRP3, Caspase-1, ASC, N-GSDMD, IL-1β, and IL-18) is presented, with data expressed as mean ± SEM; *P < 0.05, **P < 0.01, ***P < 0.001, n = 4. (K) Immunofluorescence staining was performed to visualize NEUN, a neuronal marker, and GSDMD within the CA1 region of the hippocampus. (J) Quantitative analysis of cells co-localizing NEUN and GSDMD is provided, with data expressed as mean ± SEM; significance is marked by *P < 0.05, n = 4. (L) Transmission electron microscopy images reveal ultrastructural alterations in hippocampal neurons, with a scale bar of 2 μm.

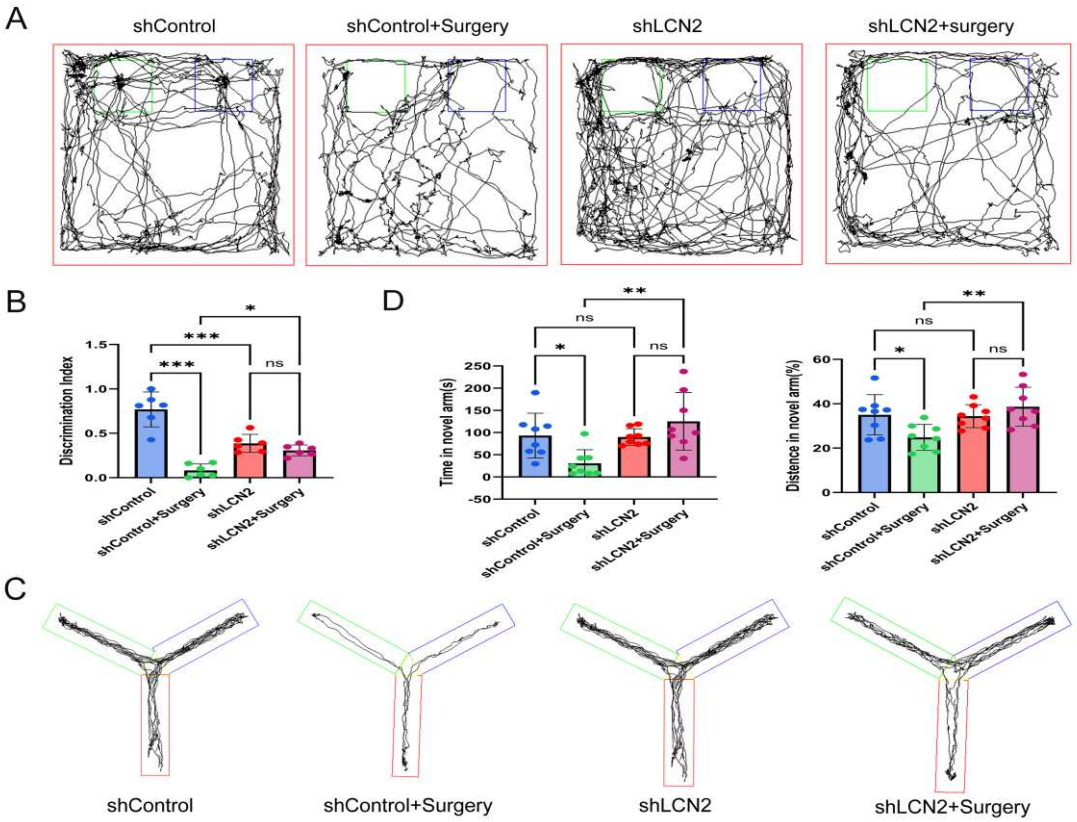


Figure 5: The knockdown of LCN2 alleviates postoperative cognitive dysfunction. (A) Exemplary movement trajectories of mice in the Novel Object Recognition (NOR) test. (B) Quantitative analysis of the recognition index in the NOR test. Data are expressed as mean ± SEM; **P < 0.01, n = 6. (C) Movement trajectories of mice in the Y-maze test. (D) Quantitative assessment of the percentage of distance and time spent exploring the novel arm in the Y-maze test; *P < 0.05, **P < 0.01, n = 6.

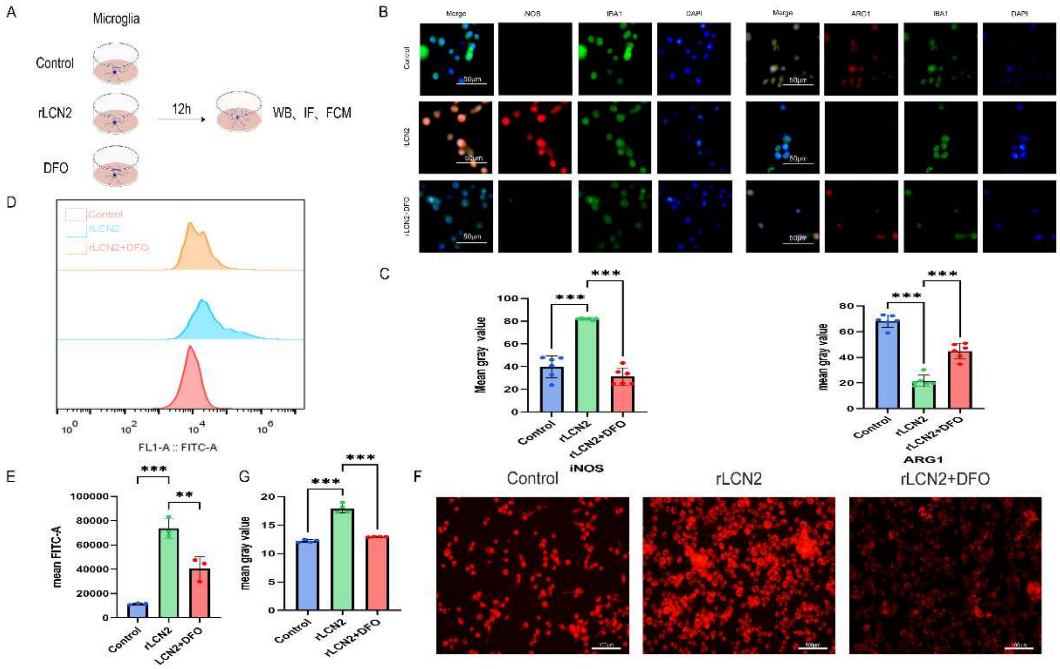


Figure 6: LCN2 Facilitates M1 Polarization of Microglia through Iron Overload and Elevated ROS Levels. (A) Schematic representation of the experimental setup. (B) Observations of fluorescence intensity changes in iNOS, ARG1, and IBA1 in polarized microglia, alongside measurements of ROS and intracellular iron levels, following a 12-hour treatment period. (C) Quantitative assessment of the mean immunofluorescence intensity of M1 polarization markers in microglia. Results are expressed as mean ± SEM; ***P < 0.001, n = 6. (D, E) Flow cytometry images and quantitative analysis of ROS levels in microglia. Results are expressed as mean ± SEM; **P < 0.01, ***P < 0.001, n = 3. (F, G) Fluorescence staining images captured via inverted microscopy and quantitative analysis of ferrous iron (Fe^{2+}) levels in microglia. Results are expressed as mean ± SEM; ***P < 0.001, n = 4.

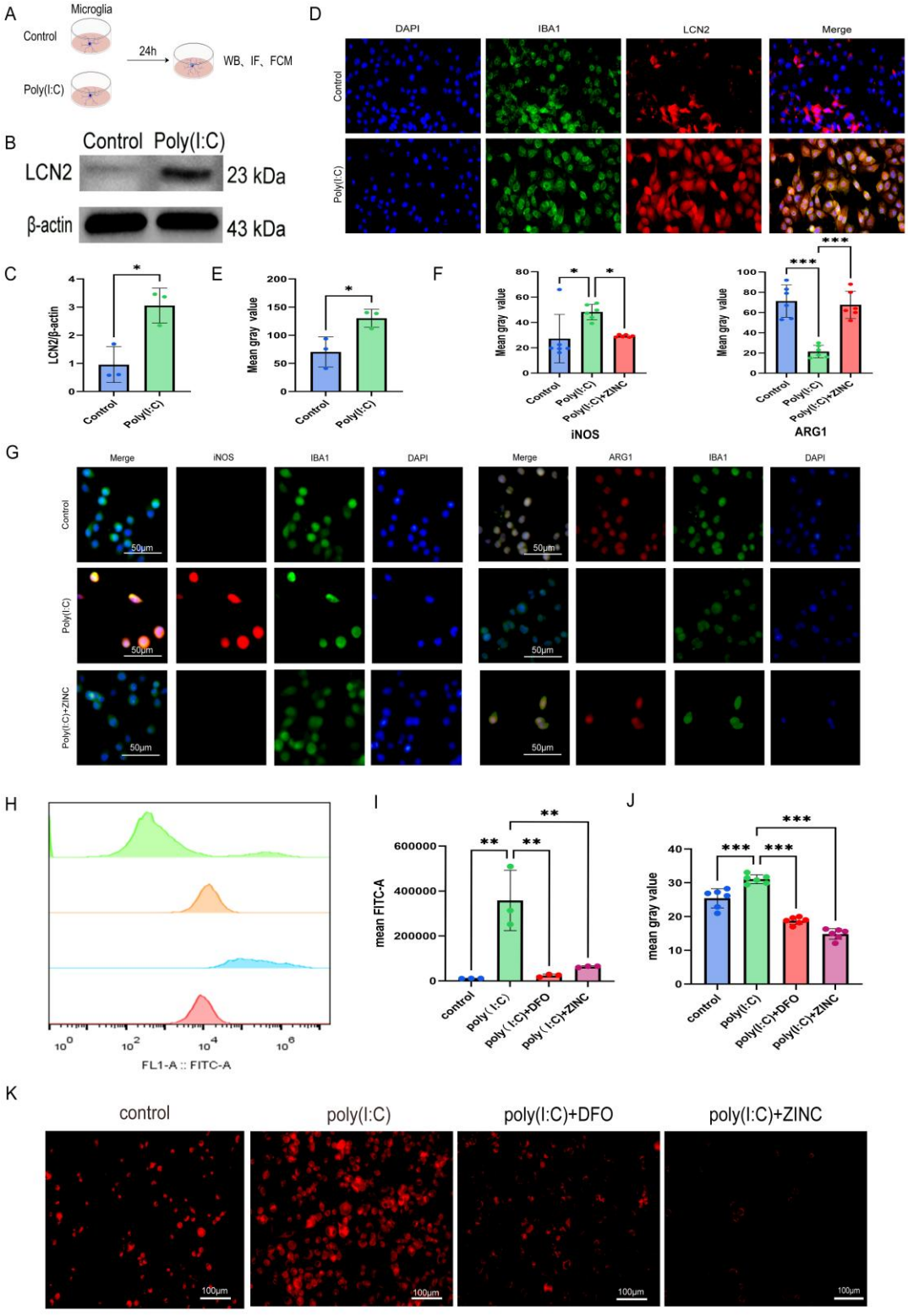


Figure 7: TLR3 Mediates Neuronal Pyroptosis via Microglial M1 Polarization. (A) Experimental Design: Microglial BV2 cells were exposed to the TLR3 agonist poly(I:C) for a duration of 24 hours. Subsequent to treatment, samples were collected for Western blotting, immunofluorescence, and flow cytometry analyses. (B, C) Western Blot

Analysis: Evaluation of LCN2 protein expression levels post poly(I:C) exposure, accompanied by quantitative assessment. Results are expressed as mean ± SEM; *P < 0.05, n = 3. (D, E) Immunofluorescence Analysis: Representative images depicting LCN2 expression in microglia, along with quantitative evaluation of LCN2-positive cells. Results are expressed as mean ± SEM; *P < 0.05, n = 3. (F, G) The images depict representative immunofluorescence staining for M1 and M2 polarization markers, specifically iNOS and ARG1, in microglia, accompanied by a quantitative assessment of the mean fluorescence intensity. The data are expressed as mean ± SEM, with significance indicated by *P < 0.05 and ***P < 0.001, based on a sample size of n=6. (H) Flow cytometry was employed to assess reactive oxygen species levels in microglia. (I) The quantitative analysis of ROS levels across the four experimental groups is presented, with data expressed as mean ± SEM and statistical significance denoted by *P < 0.05 and **P < 0.01, with n=3. (J) The images illustrate representative fluorescence staining of intracellular iron levels in microglia. (K) A quantitative analysis of the mean fluorescence intensity for intracellular iron levels is provided, with significance indicated by ***P < 0.001, based on n=6.

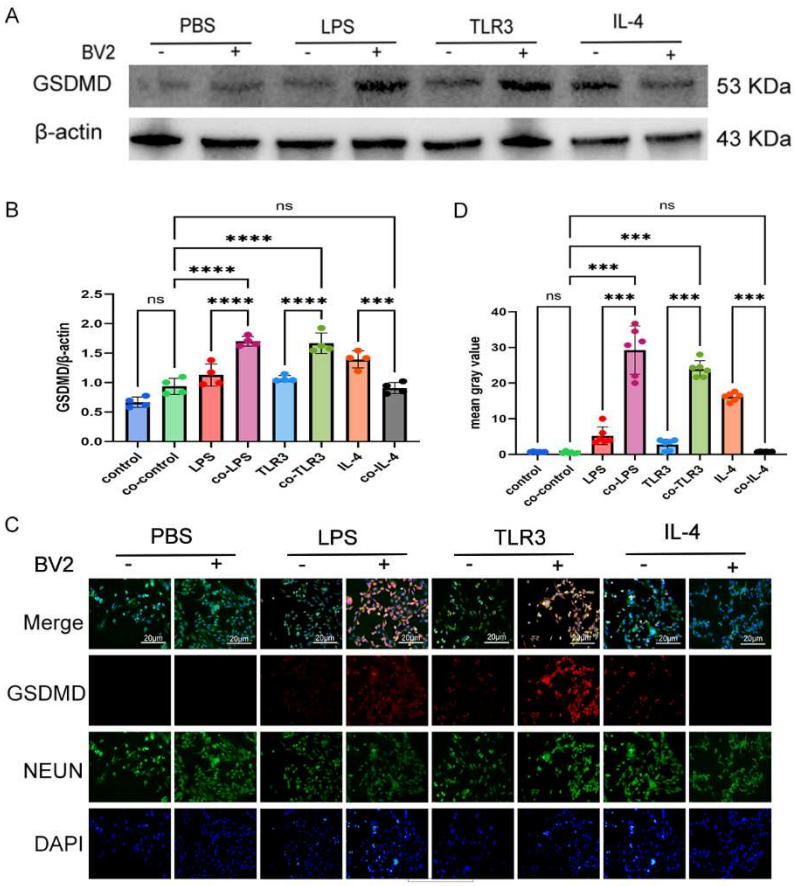


Figure 8: TLR3 facilitates neuronal pyroptosis by inducing M1 polarization in microglia. (A, B) Western blot analysis and corresponding quantification of GSDMD protein expression levels are presented. Statistical significance is indicated as follows: *P < 0.05, **P < 0.01, ***P < 0.001, with a sample size of n=4. (C, D) Representative immunofluorescence images depicting GSDMD and NEUN for each experimental group are shown, accompanied by quantitative analysis of the mean fluorescence intensity. Statistical significance is denoted by ***P < 0.001, while 'ns' indicates no significant difference, with a sample size of n=6.

Supplementary Files

This is a list of supplementary files associated with this preprint. Click to download.

- Supplementarymaterial.rar